Cooperative Motor-Thruster Vertical Orientation Control for Suspended Modules in Modular Construction Assembly

Yuxuan Lan[1], Xiao Li[1], Ruiqi Jiang[1], Shichen Sun[1]

[1] CI^3 Lab, Department of Civil Engineering, The University of Hong Kong, HK SAR, China

lucas.lan@connect.hku.hk, shell.x.li@hku.hk, richj233@connect.hku.hk, u3013991@connect.hku.hk

Abstract -

The on-site assembly of prefabricated modules relies heavily on manual labor. However, it's inefficient and exposes workers to significant safety risks, remaining a major bottleneck for modular construction (MC) assembly. This paper proposes a cooperative motor-thruster vertical orientation control system (CM-TVOCS) for suspended modules during lifting and positioning. A rotary motor system integrated at the crane hook and a distributed thruster array mounted on the lifting frame achieve both accurate, energy-efficient rotation and avoid unsafe hook constraints. Besides, a dynamic model of the suspended lifting system is established, and a hierarchical control strategy is developed for the time-optimal control. Experimental results demonstrate that the proposed system significantly outperforms single-actuator methods, achieving up to a 70% improvement in rotational accuracy with a maximum tracking error below 4.74%. The proposed approach provides a practical solution to enhance automation, precision, and safety for on-site MC assembly.

Keywords -

Cooperative Orientation Control; Crane Lifting; Dynamic Modeling; Modular Construction

1 Introduction

Modular Construction (MC) is a highly industrialized building production method that improves construction efficiency and quality by prefabricating modules in factories and transporting them to the construction site for assembly [1, 2, 3, 4]. It is particularly suitable for high-density cities, e.g., Hong Kong, where land resources are limited [5, 6]. Despite the introduction of automated robots into factories, the on-site phase of MC, especially the lifting and position process, still relies heavily on manual operations [7, 8, 9].

Among on-site operations, the vertical orientation control of suspended modules is one of the most critical and hazardous tasks. As shown in Fig. 1, when an MC module is lifted from the transportation vehicle and maneuvered to its target position, uncontrolled rotational motions may occur due to external disturbances, flexible suspension, and center-of-gravity offsets, posing a collision risk with surrounding structures [10]. In current practice, multiple guide ropes are manually attached to the module frame, and several workers pull them to control the orientation of the suspended module during lifting and positioning.

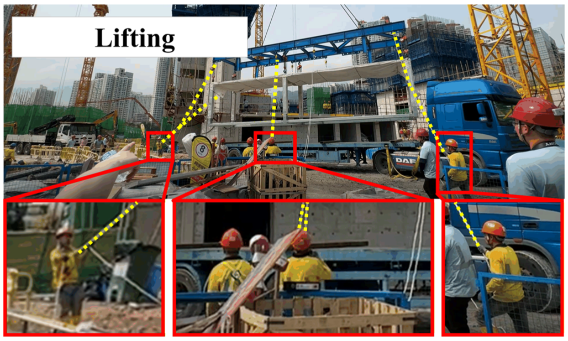

(a) Manual intervention during module lifting from the transportation vehicle

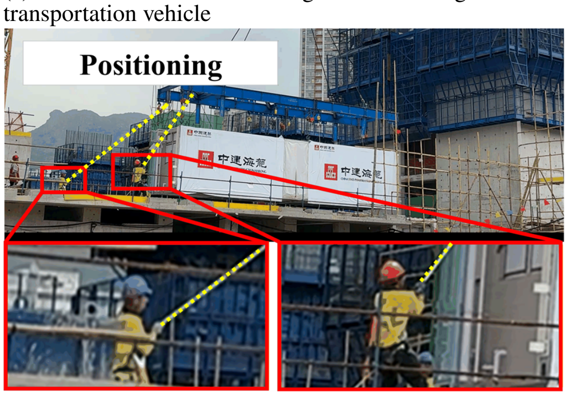

(b) Manual orientation adjustment and positioning during module installation

Figure 1. Manual vertical orientation control of MC modules during on-site assembly operations.

However, the manual orientation control process is not only inefficient but also exposes workers to significant safety hazards, particularly when lifting large, high-inertia modules in congested site environments [11]. This bottleneck motivates the development of reliable automated orientation control methods.

Although many potential orientation control strategies in other engineering domains have been developed and validated, their direct adoption for on-site MC assembly is underexplored. One key challenge of the suspended nature of MC modules is connected to the crane solely through the hook-cable system. Together with the large inertia of modules and the dynamics of cables, these factors fundamentally alter the effective torque transmission mechanism, rendering established approaches ineffective or impractical for MC.

(1) Momentum-wheel-based systems, widely adopted in aerospace applications [12], provide non-contact actuation through angular momentum exchange and have been explored in a limited number of lifting scenarios [13]. However, their substantial mass and inertia, especially when scaled for heavy payloads, pose risks of actuator saturation and high power consumption, making them impractical for routine MC operations.

(2) Conventional gearbox-based transmission systems can reliably deliver high torque [14, 15], however, effective torque transmission requires a mechanically constrained hook interface to provide a reaction torque path. In MC environments, mechanically locking the crane hook introduces unacceptable safety risks, as it restricts passive load release and amplifies the consequences of unexpected disturbances. When the hook is left unconstrained to maintain operational safety and flexibility, the transmitted torque is limited by static friction at the hook-cable interface. Although such friction can be effectively engaged and regulated by a rotary actuator, the achievable torque margin remains insufficient for MC modules.

(3) Thruster-based systems generate control torque via distributed propulsive forces [16], offering fast response and flexible deployment [17]. However, in heavy-lifting scenarios, thrusters must directly overcome passive friction torques and aerodynamic disturbances at the hook-cable interface, thereby significantly increasing the required control effort. Combined with inherent limitations in thrust capacity and power efficiency, this limits their effectiveness in achieving stable, precise orientation control for MC modules.

To address these limitations, this study proposes a cooperative motor-thruster vertical orientation control system (CM-TVOCS) that integrates a rotary actuator with a distributed thruster system for suspended MC modules. The rotary actuator primarily uses static friction for low-speed rotation, enabling precise, energy-efficient torque transmission without mechanical hook locking. In contrast, the distributed thruster compensates for rapid and auxiliary torque, which exceeds the actuator's torque margin. By exploiting these complementary features, the proposed CM-TVOCS can achieve both accurate and energy-effective rotation and avoid unsafe hook constraints.

The main contributions are summarized as follows:

(1) A CM-TVOCS is proposed for modular construction modules, introducing a dual-actuation strategy that enables safe crane operation without mechanically constraining the hook.

(2) A high-fidelity model is created for the system, accurately predicting system behavior with trajectory errors below 3.5%, and aiding in controller parameter tuning to ensure safety and efficiency during on-site implementation.

(3) A hierarchical motion control framework is proposed to coordinate the motor and thruster actuation, integrating standard control elements within a system-level architecture that enables precise and energy-efficient orientation control.

The remainder of this paper is organized as follows. Section 2 presents the nonlinear dynamic modeling of the suspended system. Section 3 introduces the hierarchical control design and torque coordination strategy. Section 4 describes the experimental setup and validation results, followed by conclusions and future work in Section 5.

2 Methodology

2.1 System Modeling

The CM-TVOCS, as illustrated in Fig. 2, comprises two main parts: the rotary motor system and the distributed thruster array. The rotary motor-bearing system consists of (1) *a slew bearing* and (2) *a rotary motor*, which is integrated into (3) *the tower-crane hook* structure, forming the upper actuation interface of the system. In addition, (4) *the distributed thruster system* composed of multiple thrusters is mounted on the MC lifting frame, enabling direct torque generation on the suspended module.

The rotary motor-bearing system and the distributed thruster system act at different locations along the suspension chain, jointly contributing to the rotational dynamics of the suspended hook-cable-frame system. This dual-actuation configuration allows rotational actuation via both the hook interface and the module body. For modeling purposes, the upper rotational components and the suspended MC module are referred to as the bearing plate and the MC module, respectively, and are denoted by subscripts p and m. The dynamic model of the suspended system is derived using the Lagrangian energy method, accounting for the interactions among the rotary actuator, thrusters, suspension cable, and module.

The lifting MC is modeled as a planar pendulum system operating at low speeds and accelerations. Its dynamics are derived via the Lagrangian formulation:

$$\frac{d}{dt}\left(\frac{\partial L}{\partial \dot{q}_i}\right) - \frac{\partial L}{\partial q_i} = Q_i \tag{1}$$

Where $L = E - U$ is the Lagrangian function, E is the total kinetic energy of the system, U is the total potential energy of the system, q_i is the generalized coordinate, and Q_i is the generalized force, $i = p, m$.

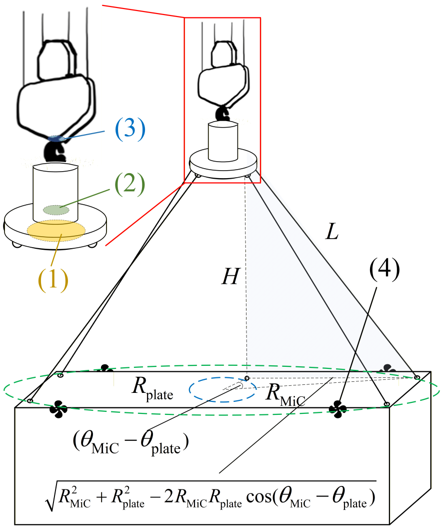

Figure 2. Structural components of the proposed suspended system

Taking the horizontal plane passing through the module's static equilibrium position as the zero-potential reference, the Lagrangian is expressed as:

$$\begin{aligned} L &= E_p + E_m - U_p - U_m \\ &= \frac{1}{2}J_p\dot{\theta}_p^2 + \frac{1}{2}J_m\dot{\theta}_m^2 - M_m g\sqrt{l + m\cos(\theta_m - \theta_p)} \end{aligned} \tag{2}$$

Where J is the moment of inertia, and the subscripts 'p' and 'm' represent the plate and the MC. $l = L_{\text{cable}}^2 - R_{\text{p}}^2 - R_{\text{m}}^2$, $m = 2R_pR_m$, L_{cable} is the cable length, R_p and R_m are the suspension radius of the plate and module, respectively, and H is the vertical distance between the slew bearing and the lifting frame.

Substituting into Eq. (1) yields the equations of motion. The generalized force Q_i encompass the motor torque, thruster force, and frictional damping, i.e., the net torque inputs into the system. The resulting dynamic equations are:

$$J_i\ddot{\theta}_i \pm \frac{M_m g\sin(\theta_m - \theta_p)}{2\sqrt{l + m\cos(\theta_m - \theta_p)}} = T_i - T_{i,\text{friction}} \tag{3}$$

The friction term is given by $T_{m,\text{friction}} = b_m\dot{\theta}_m$, $T_{p,\text{friction}} = b_p\dot{\theta}_p$, where b_m and b_p represent the motor's viscous friction coefficient and the module's aerodynamic drag coefficient. Define the state vector as:

$$\mathbf{x} = [x_1, x_2, x_3, x_4]^T = \left[\theta_m, \dot{\theta}_m, \theta_p, \dot{\theta}_p\right]^T \tag{4}$$

The state-space formula of the system is:

$$\begin{cases} \dot{x}_1 = \dot{\theta}_m \\ \dot{x}_2 = \dfrac{T_m - T_{m,\text{friction}}}{J_m} + \dfrac{gM_m\sin(\theta_m - \theta_p)}{2J_m\sqrt{l + m\cos(\theta_m - \theta_p)}} \\ \dot{x}_3 = \dot{\theta}_p \\ \dot{x}_4 = \dfrac{T_p - T_{p,\text{friction}}}{J_p} - \dfrac{gM_m\sin(\theta_m - \theta_p)}{2J_p\sqrt{l + m\cos(\theta_m - \theta_p)}} \end{cases} \tag{5}$$

2.2 Trajectory Planning

To achieve optimal control, a model-based time-optimal control method is proposed for the CM-TVOCS, optimizing rotational time while accounting for physical constraints. The nonlinear model of the system obtained in Section 2.1 is expressed as $\dot{\mathbf{x}} = f(\mathbf{x}, \mathbf{u})$, where $\mathbf{u}$ denotes the generalized torque input. The time-optimal trajectory planning problem can then be formulated as: determine the control input $\mathbf{u}^*(t)$ and the corresponding state trajectory $\mathbf{x}^*(t)$ that minimizes the time T from an initial state $\mathbf{x}_0$ to a target state $\mathbf{x}_f$, while satisfying the system dynamics and prescribed constraints:

$$\begin{aligned} &\min J = T \\ &\text{subject to:} \\ &\quad \mathbf{x}(t) = f(\mathbf{x}(t), \mathbf{u}(t)), \quad t \in [0, T] \\ &\quad \mathbf{x}(0) = \mathbf{x}_0, \quad \mathbf{x}(T) = \mathbf{x}_f \\ &\quad \mathbf{u}_{\text{min}} \le \mathbf{u}(t) \le \mathbf{u}_{\text{max}} \\ &\quad \mathbf{x}_{\text{min}} \le \mathbf{x}(t) \le \mathbf{x}_{\text{max}} \end{aligned} \tag{6}$$

The subscripts 'min' and 'max' represent the minimum and maximum allowable values of the variable. Specifically, the above constraints include two parts. The first part is the control input constraints, ensuring the z-axis motor's maximum torque satisfies $|T_{\text{p}}(t)| \le T_{\text{p, max}}$, and the thruster's maximum torque satisfies $|T_{\text{m}}(t)| \le T_{\text{m, max}}$. The second part is the system state constraints, ensuring the maximum angular velocities of the plate and MC, $|\dot{\theta}_{\text{p}}(t)| \le \dot{\theta}_{\text{p, max}}$, $|\dot{\theta}_{\text{m}}(t)| \le \dot{\theta}_{\text{m, max}}$. The maximum angular accelerations, $|\ddot{\theta}_{\text{p}}(t)| \le \ddot{\theta}_{\text{p, max}}$, $|\ddot{\theta}_{\text{m}}(t)| \le \ddot{\theta}_{\text{m, max}}$, and the maximum angular jerks, $|\dddot{\theta}_{\text{p}}(t)| \le \dddot{\theta}_{\text{p, max}}$, $|\dddot{\theta}_{\text{m}}(t)| \le \dddot{\theta}_{\text{m, max}}$. Additionally, it is necessary to ensure that the angle difference between the plate and the MC module is not too large, $|\theta_{\text{p}}(t) - \theta_{\text{m}}(t)| \le \Delta\theta_{\text{max}}$. This paper employs Pontryagin's minimum principle for trajectory planning [18]. First, we define the Hamiltonian function and the costate equation:

$$H(\mathbf{x}, \mathbf{u}, \lambda) = 1 + \lambda^T f(\mathbf{x}, \mathbf{u}), \quad \dot{\lambda} = -\frac{\partial H}{\partial \mathbf{x}} \tag{7}$$

Where λ is the costate vector, with the same dimension as the state vector $\mathbf{x}$. For this system, where $\mathbf{u}$ appears linearly, the Hamiltonian is linear in $\mathbf{u}$, implying that the optimal control is of the Bang-Bang type, meaning the control input mostly switches between its upper and lower limits, i.e.:

$$\mathbf{u}^*(t) = \arg\min_{\mathbf{u}} H(\mathbf{x}^*(t), \mathbf{u}, \lambda^*(t)) \tag{8}$$

Since the terminal time T is free, condition requires:

$$H(\mathbf{x}^*(T), \mathbf{u}^*(T), \lambda^*(T)) = -1 \tag{9}$$

To satisfy jerk limits, *smooth S-curve transitions* are inserted at bang-bang switching points. The velocity profile comprises seven phases: positive-jerk rise, constant acceleration, positive-jerk fall, constant velocity, negative-jerk rise, constant deceleration, and negative-jerk fall.

The planned optimal trajectory is discretized and stored as a lookup table containing the time-optimal state trajectory $\mathbf{x}^*(t)$ and the minimum time T^*. During online operation, the reference state $\mathbf{x}_{\text{ref}}(t)$ at the current time t obtained via the trajectory table and linear interpolation. The feedback controller then computes the feedback control $\mathbf{u}_{\text{fb}}(t)$ from the error between $\mathbf{x}_{\text{ref}}(t)$ and the measured state $\mathbf{x}(t)$.

2.3 Control Method

This section employs a multi-layer hierarchical control (MLHC) method (Fig. 3a), with its pseudo-code provided in Fig. 3b. The **trajectory planner** generates the time-optimal reference trajectory. In the cooperative actuation framework, the motor provides the primary torque for steady rotation due to its higher energy efficiency, while the thruster array generates auxiliary torque to compensate for transient dynamics and disturbance rejection.

The **system controller** integrates the position and velocity loops. The position loop employs a gain-scheduled PID controller that adjusts the proportional and derivative gains based on the plate-module angle error, balancing rapid response with smooth settling. Position and velocity are denoted as *pos* and *vel*.

$$e_{\text{pos},i}(t) = \theta_{\text{ref},i}(t) - \theta_i(t) \tag{10}$$

$$\dot{\theta}_{\text{ref},i}(t) = K_{\text{pos,p},i} \cdot e_{\text{pos},i}(t) + K_{\text{pos,i},i} \cdot \int e_{\text{pos},i}(\tau)\, d\tau + K_{\text{pos,d},i} \cdot \frac{de_{\text{pos},i}(t)}{dt} \tag{11}$$

where $e_{\text{pos},i}(t)$ is the position error, $\theta_{\text{ref},i}(t)$ is the reference position, $\theta_i(t)$ is the actual position; $\dot{\theta}_{\text{ref},i}(t)$ is the reference angular velocity output to the velocity loop; $K_{\text{pos,p},i}$, $K_{\text{pos,i},i}$, $K_{\text{pos,d},i}$ are the proportional, integral, and derivative gains of the position loop. Similarly, the speed loop uses a PID controller to calculate the control value of the actuator:

$$e_{\text{vel},i}(t) = \dot{\theta}_{\text{ref},i}(t) - \dot{\theta}_i(t) \tag{12}$$

$$u_i(t) = K_{\text{vel,p},i} \cdot e_{\text{vel},i}(t) + K_{\text{vel,i},i} \cdot \int_0^t e_{\text{vel},i}(\tau)\, d\tau + K_{\text{vel,d},i} \cdot \frac{de_{\text{vel},i}(t)}{dt} \tag{13}$$

where $e_{\text{vel},i}(t)$ is the velocity error, $\dot{\theta}_i(t)$ is the actual angular velocity; $u_i(t)$ is the final control value; $K_{\text{vel,p},i}$, $K_{\text{vel,i},i}$, $K_{\text{vel,d},i}$ are the gains of the velocity loop.

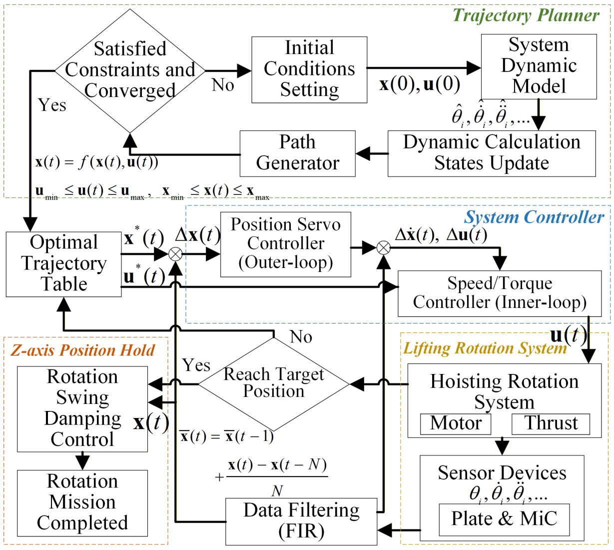

(a) Multi-layer hierarchical control architecture

```
Algorithm : Multi-Layer Hierarchical Control (MLHC) Method
  Input: Initial conditions: x_0, u_0, system dynamic model parameters
  Output: Optimal trajectory and control outputs for the system
Trajectory Planner:
TrajectoryPlanner() Set initial conditions: x_0, u_0;
while not satisfied_constraints_and_converged(x_t, u_t) do
    Update system states: θ_i, θ̇_i using SystemDynamicModel;
    Generate path: x_t, u_t from PathGenerator;
    if not converged then
        Return to Initial Conditions and restart;
Generate OptimalTrajectoryTable(x_t, u_t);
System Controller:
SystemController() Compute position error: Δx_t = x_t − x_desired;
while not reached_target_position(x_t) do
    Execute position servo control: Δx_t using PositionServoController;
    Compute speed/torque control outputs: Δẋ_t, Δu_t using
      SpeedTorqueController;
    Update HoistRotationSystem with control:
      u_t = FHoistRotation(Δu_t);
if position reached then
    Execute Z-axis position hold: x_t;
    Apply RotationSwingDampingControl;
Lifting Rotation System:
HoistRotationSystem() Generate motor and thrust commands from
  control inputs: u_t;
Retrieve sensor data: θ_i, θ̇_i;
Apply filtering to sensor data: FilteredData = FIRFilter(sensorData);
Return updated control outputs: motor, thrust;
```

(b) Pseudo-code of the control algorithm

Figure 3. Multi-layer hierarchical control method of the rotational system

The **lifting rotation system** represents the physical plant, where an IMU measures real-time states (angle, angular velocity), and the control commands are translated into coordinated motor and thruster torques. The *z-axis position hold* monitors the system's approach to the target. Once the position error falls within a preset tolerance, the controller switches to a holding mode that applies small compensatory torques to suppress post-settling oscillations caused by disturbances such as wind.

The actuator layer incorporates safety logic that triggers a safe mode upon detecting abnormal states or actuator saturation. A filter is added in the feedback path to attenuate sensor noise and high-frequency disturbances; its cutoff frequency is tuned to preserve system bandwidth while filtering noise.

3 Experiment Validation

3.1 Simulation and Experiment Setup

Before conducting engineering prototype, fine-tuning of controller parameters is necessary to obtain optimal settings and ensure safety. This section builds a high-fidelity model(Fig. 4), based on the actual dimensions of the lifting MC module, serving as a reference for parameter adjustment before deploying the on-site prototype control algorithm.

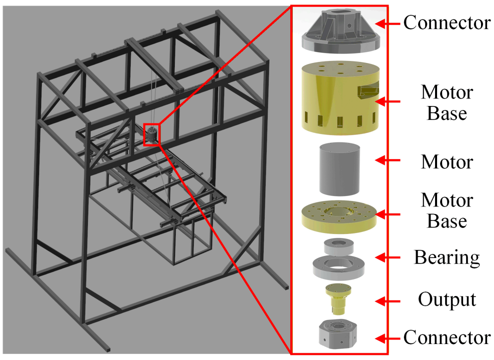

Figure 4. Physical model of suspended lifting system

Rigid body models of the bearing platform (plate) and lifted MC module are created using geometric and inertial parameters, including the mass properties of the slew bearing and the distributed mass of the MC module. Simulation parameters are listed in Table 1 based on the actual system scale-down.

Table 1. Parameter setting for the lifting system simulation model

Parameter Name	Value	Unit
Plate Moment of Inertia	0.05	$kg{\cdot}m^2$
MC Moment of Inertia	15	$kg{\cdot}m^2$
MC Module Mass	50	kg
Cable Length	1.5	m
Plate Suspension Radius	0.03	m
MC Suspension Radius	0.7	m
Max Velocity	6	deg/s
Max Acceleration	1	deg/s^2
Max Jerk	0.5	deg/s^3
Max Angle Diff (p-m)	3	deg
Position Loop Gains	[15,0,2]	/
Velocity Loop Gains	[4000,0,30]	/

The same PID controller parameters are applied to both the motor and thruster systems, tuned through a layered strategy. Additionally, due to the motor's internal communication protocol, its output control signal is uniformly scaled by a factor of 0.0165. Based on the method elaborated above, the experimental platform shown in Fig. 5 is constructed to emulate on-site lifting conditions.

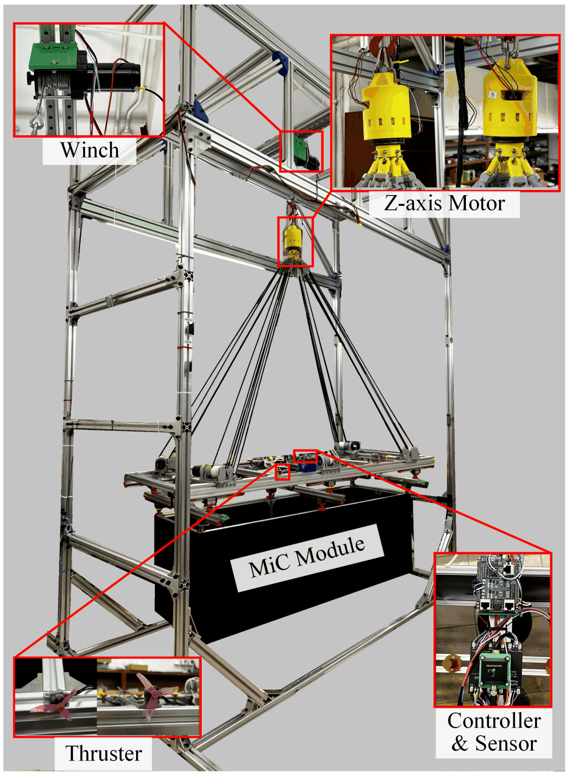

Figure 5. Experimental platform of the suspended lifting system

Key components include: a winch simulating the tower-crane trolley for vertical motion; a servo motor (z-axis motor) attached to the slew bearing outer ring, with its reducer output fixed to the inner ring for rotation; a thruster system employing brushless motors with 38.1mm blades, symmetrically mounted on the frame to directly exert rotational torque on the module; an STM32F4-based controller that sends commands to actuators and receive sensor data; an IMU gyroscope providing real-time yaw angle and angular velocity; and a Wi-Fi module enabling wireless User Datagram Protocol (UDP) communication between the host PC and the local controller for status monitoring and command transmission.

Three configurations are tested: single thruster, single motor, and the proposed CM-TVOCS. Several rotational tasks are evaluated.Evaluation criteria include MAE and RMSE of MC yaw position. Four trajectories are examined: (1) *0–60°*; (2) *0–90°*; (3) *0–120°*; (4) *0–30–100–60°*. For results demonstration, the following notation is adopted: '*c*'- command, '*mt*' - proposed CM-TVOCS, '*sm*' - single-motor method, '*st*' - single-thruster method, '*e*' - experiment, '*sim*' - simulation. Acceleration and torque are denoted *acc* and *torq*, respectively.

3.2 Simulation Results

Simulation tests show that the model closely matches the behavior of the real equipment for the specified rotational tasks.

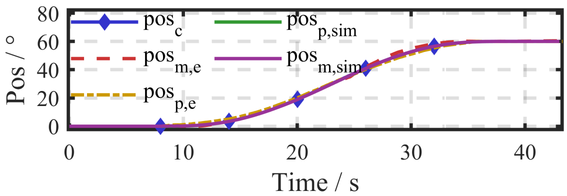

Figure 6. Suspended system angle position

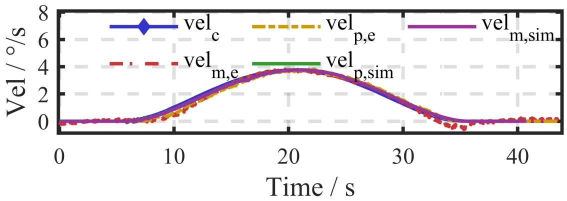

Figure 7. Suspended system angle velocity

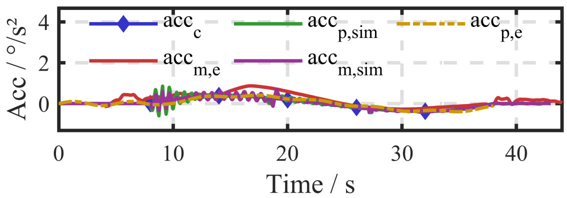

Figure 8. Suspended system angle acceleration

The MAE and RMSE between the MC position for the experiment and simulation are shown in Table 2. The trajectory error stays below 3.5%, confirming the model's accuracy.

Table 2. Simulation modeling errors

Parameter name	MAE	RMSE
Position	0.6561	0.9601
Velocity	0.1366	0.1922
Acceleration	0.2354	0.3387

This demonstrates that the model can be used to predict the actual engineering prototype, reduce parameter adjustment time, and address safety concerns during on-site debugging.

3.3 Experiment Results

This section analyzes experimental data from several tasks. First, system response is assessed using a step signal, with stability defined as maintaining angular error below 1° for at least 3 seconds. Results (Fig. 9) show that the proposed CM-TVOCS reduces oscillations compared to single-motor scheme, cutting stabilization time by 44.8% and achieving a smoother rotation.

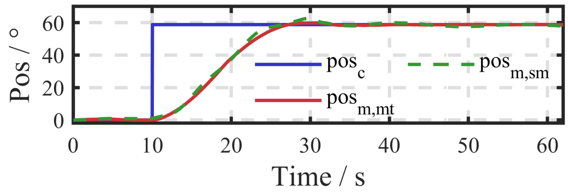

Figure 9. Position response of the step signal

The results show that the CM-TVOCS achieves superior tracking accuracy. The MAE and RMSE of the MC position under the two methods are shown in Table 3. Each CM-TVOCS experimental configuration was repeated three times under identical initial conditions to evaluate repeatability, and the MAE and RMSE in the table represent the average values from the three trials.

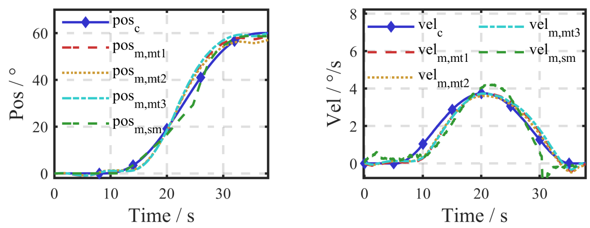

(a) MC position (b) MC velocity

Figure 10. Trajectory 1: mt vs. sm

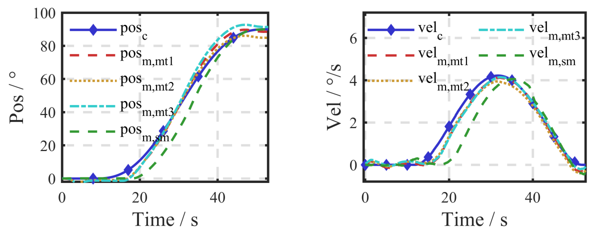

(a) MC position (b) MC velocity

Figure 11. Trajectory 2: mt vs. sm

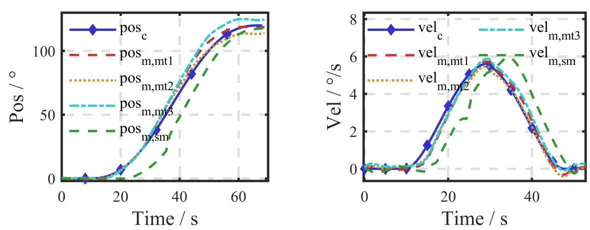

(a) MC position (b) MC velocity

Figure 12. Trajectory 3: mt vs. sm

The results indicate that the proposed method improves positioning accuracy by up to 70% compared to a traditional single-motor system.

Table 3. Position control performance for different trajectories

Method	Trajectory	MAE	RMSE
Proposed method	1	1.2175	2.0223
	2	1.5549	1.9518
	3	1.5983	2.5248
Single motor	1	1.9436	2.5194
	2	4.4023	6.1361
	3	8.2051	11.6298

Additionally, tests with single-thruster configuration, shown in Fig. 13, reveal that torque saturation prevents the thrusters from overcoming motor and slew bearing friction, causing the module to stall under maximum torque.

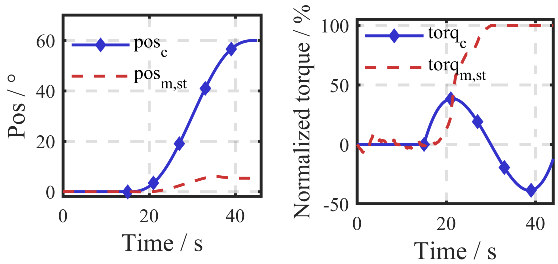

(a) MC position (b) Thruster torque

Figure 13. Single-thruster rotational control results

This indicates that the proposed method requires only moderate thruster force - specifically, less than 50% full power - to achieve rotational tasks. A complete reciprocating rotational task is conducted to evaluate the CM-TVOCS. As shown in Fig. 14 and Fig. 15, the two methods follow the planned trajectory with a maximum error of 4.74% and 12.44% (the ratio between the peak absolute yaw error and the commanded rotation angle).

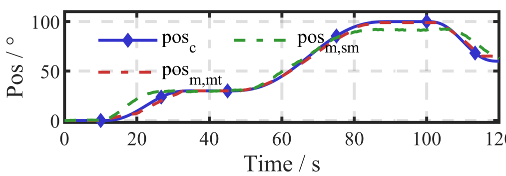

Figure 14. MC position for trajectory 4

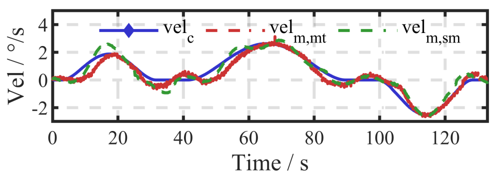

Figure 15. MC velocity for trajectory 4

4 Conclusion

This paper presented a CM-TVOCS for precise rotational regulation of suspended modules during MC assembly. By integrating a rotary motor at the crane hook with a distributed thruster array mounted on the lifting frame, the proposed system exploits the complementary features of high-precision motor actuation and fast-response thrust-based torque generation, enabling effective orientation control without mechanically constraining the crane hook.

A high-fidelity dynamic model of the suspended hook-cable-module system was established with the Lagrangian formulation, capturing the key effects of module inertia and suspension dynamics on torque transmission. Based on this model, a hierarchical control framework incorporating time-optimal trajectory planning and closed-loop feedback control was developed to coordinate motor and thruster actuation. Experimental results demonstrated that the proposed system significantly outperforms single-actuator solutions, achieving up to a 70% improvement in rotation accuracy while maintaining a maximum tracking error below 4.74%. The CM-TVOCS reduced stabilization time relative to the single-motor configuration and mitigated torque saturation observed in the single-thruster configuration.

The proposed system is compatible with standard tower crane infrastructure and requires no structural modifications to the crane, enabling rapid deployment in real construction environments. By reducing manual intervention during module lifting and positioning, the system offers a practical pathway to improving safety, precision, and operational consistency in on-site MC assembly.

Several limitations remain in this study. The current implementation focuses on planar rotational motion about the vertical axis to isolate the core orientation control problem. Factors such as cable elasticity and large wind disturbances were not explicitly modeled. In full-scale deployment, higher-power thrusters or alternative force generators may be adopted. Future work will address these limitations and extend the framework to full three-dimensional attitude regulation and multi-module cooperative assembly under realistic construction conditions.

Acknowledgment

This research was supported by grants from the Hong Kong Innovation and Technology Fund (Reference No. PRP-048-24LI) and the China State Hailong Construction Technology Limited; and was also supported by RISUD, PolyU (P0052942).

References

[1] W. Ferdous, Y. Bai, T. Manalo, et al. New advancements, challenges and opportunities of multi-storey modular buildings – a state-of-the-art review. *Engineering Structures*, 183:883–893, 2019. doi:10.1016/j.engstruct.2019.01.061.

[2] S. Abdelmageed and T. Zayed. A study of literature in modular integrated construction - critical review and future directions. *Journal of Cleaner Production*, 277:124044, 2020. doi:10.1016/j.jclepro.2020.124044.

[3] Y. W. Lim, P. C. H. Ling, C. S. Tan, and H. Y. Chong. Planning and coordination of modular construction. *Automation in Construction*, 141:104455, 2022. doi:10.1016/j.autcon.2022.104455.

[4] Buildings Department. Code and references for modular integrated construction hong kong. On-line: `https://www.bd.gov.hk/tc/resources/codes-and-references/modular-integrated-construction/index.html`, Accessed: 29/07/2025.

[5] X. Zhao, T. Zayed, and Y. Niu. Comparative analysis of modular construction practices in mainland china, hong kong and singapore. *Journal of Cleaner Production*, 245:118861, 2020. doi:10.1016/j.jclepro.2019.118861.

[6] Y. Zhang, S. Chen, and W. Pan. Systematic initial embodied carbon assessment of concrete modular high-rise residential buildings: A case in hong kong. *Building and Environment*, 265:111917, 2024. doi:10.1016/j.buildenv.2024.111917.

[7] C. Song, X. Li, Q. Du, et al. Hybrid pose adjustment (hypa) robot design for prefabricated module control in modular construction assembly. *Automation in Construction*, 168(A), 2024. doi:10.1016/j.autcon.2024.105798.

[8] S. M. Bagheri, H. Taghaddos, and U. Hermann. Automated safety and practicality enhancement of lift plans in modular construction. *Automation in Construction*, 168:105731, 2021. doi:10.1016/j.autcon.2024.105731.

[9] S. F. Abdulai, T. Wuni, I. Y. Antwi, et al. Cross-industry review of autonomous alignment technologies: Adaptation potential for modular construction. *Journal of Cleaner Production*, 495:145101, 2025. doi:10.1016/j.jclepro.2025.145101.

[10] A. Zhu, Z. Zhang, and W. Pan. Developing a fast and accurate collision detection strategy for crane-lift path planning in high-rise modular integrated construction. *Advanced Engineering Informatics*, 61:102509, 2024. doi:10.1016/j.aei.2024.102509.

[11] Z. Lei, S. Han, A. Bouferguène, et al. Algorithm for mobile crane walking path planning in congested industrial plants. *Journal of Construction Engineering and Management*, 141(2), 2020. doi:10.1061/(ASCE)CO.1943-7862.0000929.

[12] K. Chen, H. Zhou, and X. Shan. Rotation-control device for construction cranes with nested pid control. *Automation in Construction*, 146:104704, 2023. doi:10.1016/j.autcon.2022.104704.

[13] Leighton Asia. Roborigger: a game changer in lifting safety. On-line: `https://www.leightonasia.com/news-centre/2024/roborigger-a-game-changer-in-lifting-safety`, 2024.

[14] Caldwell. Motorized rotating crane hook clevis style. On-line: `https://www.caldwellinc.com/products/strong-bac/rotating-crane-hooks/Model-50`, 2025.

[15] X. Kong, Z. Hu, J. Chen, et al. Effects of gear flexibility on the dynamic characteristics of spur and helical gear system. *Mechanical Systems and Signal Processing*, 184:109691, 2023. doi:10.1016/j.ymssp.2022.109691.

[16] S. J. Lee, D. Lee, J. Kim, et al. Fully actuated autonomous flight of thruster-tilting multirotor. *IEEE/ASME Transactions on Mechatronics*, 26(2):765–776, 2021. doi:10.1109/TMECH.2020.2999586.

[17] D. Angelis, L. Emanuele, and G. Fabrizio. Stability and control issues of multirotor suspended load transportation: An analytical closed–form approach. *Aerospace Science and Technology*, 135: 108201, 2023. doi:10.1016/j.ast.2023.108201.

[18] W. Jin, Z. Wang, Z. Yang, et al. Pontryagin differentiable programming: An end-to-end learning and control framework. *Advances in Neural Information Processing Systems*, 33:7979–7992, 2020. doi:10.48550/arxiv.1912.12970.